

# Signatures of topology in quantum quench dynamics and their interrelation

Lorenzo Pastori, Simone Barbarino, and Jan Carl Budich

*Institute of Theoretical Physics, Technische Universität Dresden,  
and Würzburg-Dresden Cluster of Excellence ct.qmat, 01062 Dresden, Germany*

Motivated by recent experimental progress in the study of quantum systems far from equilibrium, we investigate the relation between several dynamical signatures of topology in the coherent time-evolution after a quantum quench. Specifically, we study the conditions for the appearance of entanglement spectrum crossings, dynamical quantum phase transitions, and dynamical Chern numbers. For non-interacting models, we show that in general there is no direct relation between these three quantities. Instead, we relate the presence of level crossings in the entanglement spectrum to localized boundary modes that may not be of topological origin in the conventional sense. Finally, we investigate how interactions influence the presence of entanglement spectrum crossings and dynamical quantum phase transitions, by means of time-dependent density matrix renormalization group simulations.

## I. INTRODUCTION

Founded on the general notion of topological phases of matter [1–3], physical phenomena reflecting topological properties by now have been predicted and observed in a broad variety of systems. While in conventional solid-state settings topological states are typically realized at low temperatures, recent advances in quantum simulators, e.g. implemented with ultra-cold atomic gases [4–6], provide new opportunities for detecting dynamical signatures of topology in quantum matter far from equilibrium [7–10]. There, an enormous tunability enables the implementation of a wide range of topological models [11–18] (see [7–9] for recent reviews), and the high degree of isolation allows for the realization of coherent quantum many-body dynamics over relatively long timescales.

A common protocol to investigate the interplay between topology and dynamics is to perform a quantum quench, where the system is initialized in a topologically trivial state that can be prepared at low entropy, before some parameters in its Hamiltonian are changed to a topological regime. In this scenario, numerous non-equilibrium signatures witnessing the change of topology have been identified [19–41], including dynamical quantum phase transitions [32–37] (DQPTs), entanglement spectrum crossings [38–40] (ESCs), and a dynamical Chern number [41] (DCN). These concepts characterize the post-quench time-evolution from quite different physical perspectives. For quench protocols within the same Altland-Zirnbauer (AZ) symmetry class [42–44], it is known that DQPTs appear as a consequence of crossing a quantum critical point between a trivial and a topological phase [33, 34, 36, 45]. By contrast, ESCs are a quantum information signature generalizing the presence of protected boundary modes in the entanglement spectrum [46–49], thus representing an instantaneous property of the time-evolved state [31]. Instead, the DCN is a topological invariant defined over a dimensionally extended space-time domain [41].

In this work, we present a comprehensive study of the relations between DQPTs, ESCs, and DCN as

fingerprints of non-equilibrium topology in quantum quench dynamics, focusing on the fully microscopic study of one-dimensional systems. We consider quantum quenches that are not necessarily restricted to a certain AZ symmetry class, and explicitly construct quench protocols exhibiting most of the possible combinations regarding the presence and absence of DQPT, ESC, and DCN (see Table I), where the absence of the few unobserved combinations is motivated with a simple geometric picture. In this sense, our results imply that there is no one-to-one correspondence between any of pair of those three signatures.

When constraining the quench protocol to a given AZ class, all three signatures individually still constitute a hallmark of some non-trivial topological properties in quench dynamics, albeit an earlier suggested direct correspondence between ESC and DCN [40] has been partly refuted [30, 31, 50]. Here, going beyond the notion of symmetry-preserving quenches, we show how these features generally are neither related to topological properties of the pre- and post-quench Hamiltonians, nor to an emergent topology of the time-evolved state. Instead, we observe how these signatures can be dynamically generated even by quenches between topologically trivial Hamiltonians, and how the ESCs can occur as a consequence of accidental boundary modes having no topological origin. Finally, by means of time-dependent density matrix renormalization group [51, 52] (DMRG) simulations, we first investigate the robustness of ESCs and DQPTs against interactions, and finally show how such signatures can appear after a quench of the interaction strength in a correlated version of the Su-Schrieffer-Heeger model [53].

This paper is structured as follows. In Sec. II, we briefly review how ESCs, DQPTs and DCN can be calculated for two-banded systems out of equilibrium. In Sec. III and IV A we present our results in the non-interacting and in the interacting regime, respectively. We finally conclude in Sec. V.

## II. MODEL AND INDICATORS OF TOPOLOGY

In this section, we introduce the general framework and notations to be used throughout this article. We consider a one-dimensional chain of spinless fermions with a number  $L$  of unit cells, each one consisting of two orbitals, or sublattice sites, labeled with  $A$  and  $B$ . We denote the fermionic operators annihilating a spinless fermion on sublattices  $A$  and  $B$  with  $\hat{a}_j$  and  $\hat{b}_j$ , respectively, where  $j = 1, \dots, L$ . In the following, we will focus on the case where the system is initially prepared in the ground state  $|\Psi\rangle$  of a pre-quench Hamiltonian  $\hat{H} = \sum_{i,j} \hat{\Pi}_i^\dagger h_{ij} \hat{\Pi}_j$ , with  $\hat{\Pi}_j^\dagger = (\hat{a}_j^\dagger \ \hat{b}_j^\dagger)$ . At time  $t = t_0$  the Hamiltonian of the system is suddenly switched to  $\hat{H}' = \sum_{i,j} \hat{\Pi}_i^\dagger h'_{ij} \hat{\Pi}_j$  such that, for  $t > t_0$ , the state of the system will be  $|\Psi(t)\rangle = \hat{U}(t)|\Psi\rangle$ , with  $\hat{U}(t) = e^{-i\hat{H}'(t-t_0)}$  being the unitary time-evolution operator. Without loss of generality we assume  $t_0 = 0$  and observe that, at each time  $t$  after the quantum quench, the time-evolved state  $|\Psi(t)\rangle$  is the ground state of a time-dependent Hamiltonian:

$$\hat{H}_P(t) = e^{-i\hat{H}'t} \hat{H} e^{+i\hat{H}'t}, \quad (1)$$

called *parent* Hamiltonian [40], which satisfies the equation of motion  $i\partial_t \hat{H}_P(t) = [\hat{H}', \hat{H}_P(t)]$  with the initial condition  $\hat{H}_P(0) = \hat{H}$ . In the following we will focus on systems with periodic boundary conditions, and the momentum state description becomes a convenient basis for the explicit calculation of the parent Hamiltonian in the two-band models considered. We introduce the momentum space operators  $\hat{a}_k = \sum_j e^{ikj} \hat{a}_j / \sqrt{L}$  and  $\hat{b}_k = \sum_j e^{ikj} \hat{b}_j / \sqrt{L}$ , with  $k = 2\pi n/L$  and  $n = -L/2, \dots, L/2 - 1$ . In this basis the parent Hamiltonian reads as  $\hat{H}_P(t) = \sum_k \hat{\Pi}_k^\dagger h_P(k, t) \hat{\Pi}_k$  where  $\hat{\Pi}_k^\dagger = (\hat{a}_k^\dagger \ \hat{b}_k^\dagger)$ , and  $h_P(k, t) = \vec{d}_P(k, t) \cdot \vec{\sigma}$ , with  $\vec{\sigma}$  being the vector of the three Pauli matrices acting in the sublattice space and  $\vec{d}_P(k, t)$  the Bloch vector characterizing  $\hat{H}_P(t)$ . The Bloch Hamiltonian  $h_P(k, t)$  for a single momentum  $k$  satisfies  $i\partial_t h_P(k, t) = [h'(k), h_P(k, t)]$ . We will consider quench protocols where the Bloch vector  $\vec{d}(k)$  characterizing the pre-quench Hamiltonian  $\hat{H}$  is changed to the vector  $\vec{d}'(k)$  characterizing the post-quench Hamiltonian  $\hat{H}'$ . For such scenario, it can be seen that the Bloch vector  $\vec{d}_P(k, t)$  is the solution of the differential equation [40, 41]:

$$\partial_t \vec{d}_P(k, t) = 2\vec{d}'(k) \times \vec{d}_P(k, t), \quad (2)$$

with initial condition  $\vec{d}_P(k, 0) = \vec{d}(k)$ . The solution to the above equation can be written as:

$$\begin{aligned} \vec{d}_P(k, t) = & \vec{d}_\parallel(k) + \cos[2d'(k)t] \vec{d}_\perp(k) + \\ & + \sin[2d'(k)t] \vec{d}_o(k), \end{aligned} \quad (3)$$

ESC	DQPT	DCN	exists (✓)/does not exist (✗)
yes	yes	yes	✓
no	yes	yes	✓
yes	no	yes	✗
no	no	yes	✗
yes	yes	no	✓
no	yes	no	✓
yes	no	no	✓
no	no	no	✓

TABLE I. Summary of our main results in the non-interacting case, showing the relations among ESCs, DQPTs, and DCN, for quenches in one-dimensional two-band models. The ✓ or ✗ for the rows mark the possibility or impossibility, respectively, of devising quench protocols featuring the corresponding combination of the three signatures in the subsequent unitary time-evolution.

where  $d(k) \equiv |\vec{d}(k)|$  and  $d'(k) \equiv |\vec{d}'(k)|$ , and:

$$\vec{d}_\parallel(k) = \frac{[\vec{d}(k) \cdot \vec{d}'(k)]}{d'^2(k)} \vec{d}'(k), \quad (4a)$$

$$\vec{d}_\perp(k) = \vec{d}(k) - \vec{d}_\parallel(k), \quad (4b)$$

$$\vec{d}_o(k) = -\frac{\vec{d}(k) \times \vec{d}'(k)}{d'(k)}. \quad (4c)$$

The parent Hamiltonian offers a way of defining the notion of non-equilibrium topology in quantum quench problems. There are two *inequivalent* definitions of it. The approach followed by [40] and [41] is that of defining the non-equilibrium topology as the  $(1+1)$ -dimensional topology of the of the parent Hamiltonian, i.e. taking time as an additional dimension. In Refs. [30, 31] instead, the topology of the time-evolved state is understood as the 1-dimensional topology of a band-flattened parent Hamiltonian, to which a classification similar to the equilibrium one is then applied. As we will emphasize in the following, for quenches within the same AZ class, looking at the DCN and the entanglement spectrum dynamics correspond to probing the two above definitions of non-equilibrium topology, respectively, while DQPTs occur for quenches crossing a quantum critical point [33, 34]. For general quantum quenches, not restricted to a given AZ class, we will show how these three signatures will become unrelated to any topology of the pre- or post-quench, or parent Hamiltonian. In the next section we review the definitions of entanglement spectrum, DQPTs and DCN, and how they can be calculated in non-interacting two-band systems.

### 1. Entanglement spectrum

The entanglement spectrum of a given Hamiltonian  $\hat{H}$  is the set of the eigenvalues  $\{\lambda_m\}$  of the reduced density matrix  $\hat{\rho}_S = \text{Tr}_{\bar{S}} |\Psi\rangle\langle\Psi|$  for a subsystem  $S$  of length

$\ell < L$ , where  $\text{Tr}_{\bar{S}}$  denotes the partial trace over the complement  $\bar{S}$  of  $S$  in the total system, and  $|\Psi\rangle$  is the quantum state of the total system. In the following, we will calculate the entanglement spectrum for the post-quench time-evolved state  $|\Psi(t)\rangle$ , choosing the subsystem  $S$  consisting of the first  $\ell = L/2$  unit cells. For non-interacting systems, the entanglement spectrum can be easily calculated from the single-particle density matrix (see e.g. Refs. [54, 55] and Appendix A 1). This allows us to access the full post-quench time-evolution of the entanglement eigenvalues  $\{\lambda_m(t)\}$  by just calculating the eigenstates of the single-particle parent Hamiltonian  $\hat{H}_P(t)$  at each time  $t$ .

For the following discussion it is important to recall that there exists a connection between the topological nature of the state and the degeneracy of the eigenvalues in the entanglement spectrum [46–49]. In particular, exponentially localized zero-energy modes in the spectrum of the Hamiltonian with open boundary conditions imply the presence of degeneracies in the entanglement spectrum, as a consequence of zero-energy entanglement modes appearing when the cut between the two subsystems  $S$  and  $\bar{S}$  is performed. A topological phase corresponds thus to a degenerate entanglement spectrum, through bulk-boundary correspondence. The presence of ESCs in the post-quench Hamiltonian, which results in a degenerate entanglement spectrum at specific instants in time, determines if the parent Hamiltonian  $\hat{H}_P(t)$ , for the system with open boundary conditions, is endowed with zero-energy modes. For quenches in the same AZ class this corresponds to probing the 1-dimensional topology of the parent Hamiltonian [30, 31]. We will see however that, for general quench protocols, ESCs may appear as a consequence of boundary modes not related to a topological phase in the standard sense.

## 2. Dynamical phase transition

A DQPT is signaled by a divergence of a rate function  $f(t)$  at a certain instant of time  $t$ , where  $f(t)$  is defined as [32]:

$$f(t) = - \lim_{L \rightarrow +\infty} \frac{1}{L} \ln[\mathcal{L}(t)], \quad (5)$$

associated to the Loschmidt echo (a return probability)  $\mathcal{L}(t) = |\langle \Psi | e^{-i\hat{H}t} | \Psi \rangle|^2$ , where  $|\Psi\rangle$  denotes the initial state, commonly chosen to be the ground state of the pre-quench Hamiltonian. For two-band systems it is possible to show that (see Appendix A 2):

$$f(t) = - \int_{-\pi}^{\pi} \frac{dk}{2\pi} \ln [\cos^2[d'(k)t] + \gamma(k) \sin^2[d'(k)t]], \quad (6)$$

where  $\gamma(k) = [\vec{n}'(k) \cdot \vec{n}(k)]^2$ ,  $\vec{n}(k) = -\vec{d}(k)/d(k)$  and  $\vec{n}'(k) = -\vec{d}'(k)/d'(k)$ . From Eq. (6) we immediately ob-

serve that DQPTs occur when  $\gamma(k^*) = 0$  for some momenta  $k^*$ . Furthermore, we notice that the expression for  $\gamma(k)$  is independent of the direction of the quench, and so is the presence of DQPTs.

A relation between DQPTs and topology was made in Refs. [33, 34], where it was shown how DQPTs would appear after quenches between Hamiltonians in different topological phases, and a dynamical topological order parameter capturing such change was introduced [34]. In the following we will also provide example of DQPTs occurring after quenches between topologically trivial Hamiltonians.

## 3. Dynamical Chern number

The dynamical Chern number is defined for non-interacting two-band models in one dimension, as the Chern number of the parent Hamiltonian in a  $(1+1)$ -dimensional momentum-time domain. The DCN associated to a generic parent Hamiltonian  $h_P(k, t) = \vec{d}_P(k, t) \cdot \vec{\sigma}$  is defined as [41]:

$$C_{\text{dyn}}^{(m)} = \int_A \frac{dk}{4\pi} \int_0^{T_k} dt \vec{n}_P(k, t) \cdot [\partial_k \vec{n}_P(k, t) \times \partial_t \vec{n}_P(k, t)], \quad (7)$$

where  $\vec{n}_P(k, t) = \vec{d}_P(k, t)/|\vec{d}_P(k, t)|$ , with  $\vec{d}_P(k, t)$  defined in Eq. (3), and  $T_k = \frac{\pi}{d'(k)}$ . The momentum interval  $A \equiv [k_m, k_{m+1}]$ , with  $m = 1, \dots, N$ , is defined by the two consecutive momenta  $k_m$  and  $k_{m+1}$  inside the first Brillouin zone  $[-\pi, \pi)$  for which  $\vec{n}(k_m) = \vec{d}(k_m)/|\vec{d}(k_m)|$  is parallel or anti-parallel to  $\vec{n}'(k_m) = \vec{d}'(k_m)/|\vec{d}'(k_m)|$ , implying that for each of the  $k_m$ ,  $\vec{d}_P(k_m, t)$  is constant in time equal to its initial value  $\vec{d}(k_m)$ . If no such fixed momenta  $k_m$  are present, the domain of integration of Eq. (7) is equivalent to a torus, since  $\vec{d}_P(\pi, t) = \vec{d}_P(-\pi, t)$  and  $\vec{d}_P(k, t + \pi/d'(k)) = \vec{d}_P(k, t)$ . In the presence of  $N$  fixed momenta  $k_m$ , the domain of integration of Eq. (7) can be decomposed into  $N$  momentum-time submanifolds, each of them having the topology of a sphere, since the Bloch states at  $k_m$  do not evolve apart from a global phase. The DCN in Eq. (7) can be conveniently expressed as [41]:

$$C_{\text{dyn}}^{(m)} = \frac{1}{2} (\cos \theta_{k_{m+1}} - \cos \theta_{k_m}), \quad (8)$$

with  $\theta_{k_m}$  being the angle between  $\vec{n}(k_m)$  and  $\vec{n}'(k_m)$ . In the special case where the quench is performed within the same symmetry class of the Altland-Zirnbauer classification, the dynamical Chern number can be related to the winding numbers (BDI and AIII symmetry class) or to the  $\mathbb{Z}_2$  topological numbers (D symmetry class) of the pre- and post-quench Hamiltonians. For general quantum quenches, we will see how a finite DCN can arise quenching between two topologically trivial Hamiltonians, thus demonstrating how this indicator could be dynamically generated also in trivial cases.

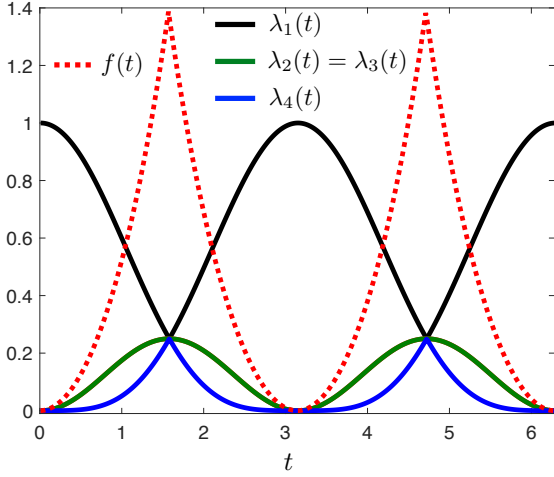


FIG. 1. Time evolution of the four largest entanglement spectrum eigenvalues (solid lines) and of the rate function  $f(t)$  (dashed red line) for the quench protocol:  $\vec{d}(k) = (J_x, 0, 0)$  and  $\vec{d}'(k) = (J_x \cos k, J_x \sin k, 0)$ . Here  $L = 1000$  sites and  $J_x = 1$ . In this case the ESCs and the DQPTs signaled by the divergences of  $f(t)$  appear at the same instants in time, while the DCN is quantized to one.

### III. NON-INTERACTING QUENCH DYNAMICS

This section is aimed at discussing the relations between DQPTs, DCNs and ESCs in non-interacting systems. First, we discuss the first four cases of Table I where the DCN is quantized and different from zero. We show that a finite quantized DCN is a sufficient condition to have a DQPT, while there is no connection between the DCN and the presence of ESCs. Then, we address the four remaining cases of Table I characterized by a vanishing DCN and we study a simple quench protocol which allows us to show that there are no connections between ESCs and DQPTs. Finally, we show that ESCs are accompanied by the appearance of zero-energy modes and discuss their topological origin. In the following, the vectors  $\vec{d}(k)$  and  $\vec{d}'(k)$  associated to the pre-quench and the post-quench Hamiltonians respectively fully determine the time-evolution of the system. As before, we set  $\vec{n}(k) = \vec{d}(k)/|\vec{d}(k)|$  and  $\vec{n}'(k) = \vec{d}'(k)/|\vec{d}'(k)|$ .

#### A. Non-vanishing dynamical Chern number

##### 1. Simultaneous presence of ESC and DQPT

We consider a system which is prepared in the ground state of a purely classical Hamiltonian and then evolves with the Su-Schrieffer-Heeger (SSH) Hamiltonian [53]. This corresponds to the case studied in Ref. [40]. We show in the following that the presence of ESCs probes in this case one-dimensional the topology of the parent

Hamiltonian  $H_P(t)$ , and that their degeneracy reflects the number of edge modes in the spectrum of  $H_P(t)$  [40]. The Bloch vectors  $\vec{d}(k)$  and  $\vec{d}'(k)$  corresponding to the pre-quench and the post-quench Hamiltonians are given by:

$$\vec{d}(k) = (J_x, 0, 0), \quad (9a)$$

$$\vec{d}'(k) = (J_x \cos k, J_x \sin k, 0), \quad (9b)$$

and are parallel and anti-parallel for  $k = 0$  and  $k = \pi$  respectively. This identifies two distinct momentum-time regions for the calculation of the DCN, and using Eq. 8 we observe that it is quantized to one (minus one) depending on which region we consider. From Eq. (3) we can also determine the Bloch vector  $\vec{d}_P(k, t)$  of the parent Hamiltonian (see Appendix (A3) for details):

$$d_P^{(x)}(k, t) = -J_x + 2J_x \sin^2(J_x t) \sin^2 k, \quad (10a)$$

$$d_P^{(y)}(k, t) = -2J_x \sin^2(J_x t) \sin k \cos k, \quad (10b)$$

$$d_P^{(z)}(k, t) = -J_x \sin^2(2J_x t) \sin k, \quad (10c)$$

which is periodic in time with the same period  $\pi/J_x$  for each  $k$ . The finite DCN reflects the presence of *skyrmion* configurations of the normalized Bloch vector  $\vec{n}_P(k, t) = \vec{d}_P(k, t)/|\vec{d}_P(k, t)|$  in half of the momentum-time zone  $[-\pi, \pi] \times [0, \pi/J_x]$ . Since the particle-hole symmetry  $C = \sigma_z \mathcal{K}$  (with  $\mathcal{K}$  being the complex conjugation) of the model is preserved in the time-evolution [30, 31],  $\vec{d}_P(k, t)$  and  $\vec{d}_P(-k, t)$  are related at all times, implying that a skyrmion with charge (Chern number) +1 in one half of the momentum-time manifold must appear together with one having charge -1 in the other half. The DCN for the total momentum-time zone is therefore zero. At times  $t^* = \pi/(2J_x) + m\pi/J_x$  the parent Hamiltonian corresponds to a next-nearest-neighbor SSH model [56], i.e.  $d_P(k, t^*) = (-J_x \cos 2k, -J_x \sin 2k, 0)$ , endowed with a chiral symmetry  $S = \sigma_z$  such that  $S h_P(k, t^*) S^\dagger = -h_P(k, t^*)$ . The time-evolution of the entanglement spectrum reflects the periodicity of the  $\vec{d}_P(k, t)$  vector. In particular, as shown in Fig. 1 (solid lines), when the parent Hamiltonian corresponds to the next-nearest-neighbor SSH Hamiltonian, the four largest eigenvalues are degenerate signaling the presence of four topological zero-energy modes. In this sense, the ESCs are topological. The winding number of the parent Hamiltonian changes from the initial value 0 to 2 at the times  $t^*$  where the ESCs happen. This is consistent with the out-of-equilibrium classification of Ref. [31], where for the BDI class in one dimension one has that the equilibrium classification  $\mathbb{Z}$  reduces to  $\mathbb{Z}_2$ . By calculating  $\gamma(k) = [\vec{d}(k) \cdot \vec{d}'(k)]^2 = J_x^4 \cos^2 k$ , we also observe that for  $k = \pi/2$  the system undergoes a DQPT at times  $t^* = \pi/(2J_x) + m\pi/J_x$ , as can be seen in Fig. 1 (dashed red line). The fact that in this example DQPTs and ESCs occur at the same times is a consequence of the post-quench Hamiltonian having flat bands. The presence of band dispersion makes the parent Hamiltonian



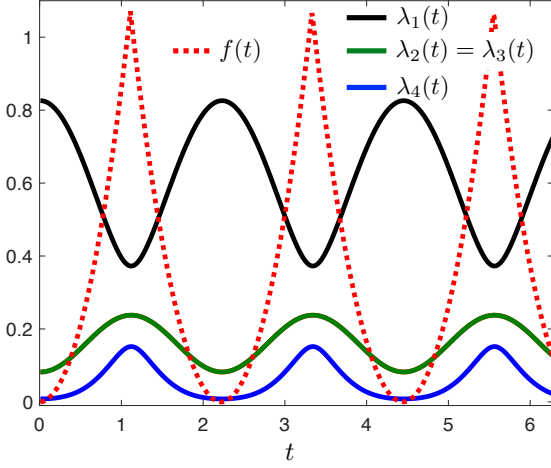


FIG. 2. Time evolution of the four largest entanglement spectrum eigenvalues (solid lines) and of the rate function  $f(t)$  (dashed red line) for the quench protocol:  $\vec{d}(k) = (J_x, 0, J_z \cos k)$  and  $\vec{d}'(k) = (J_x \cos k, J_x \sin k, J_z)$ . Here  $L = 1000$ ,  $J_x = 1$  and  $J_z = 1$ . In this case, the presence of DQPTs is not accompanied by ESCs, while the DCN is quantized to one.

not periodic in time anymore, and shifts the instants at which DQPTs occur away from the ESCs. This already hints to the fact that DQPTs and ESCs are unrelated.

### 2. Absence of ESCs and presence of DQPTs

In order to show that a finite DCN does not imply the presence of crossings in the entanglement spectrum, we consider a quantum quench determined by:

$$\vec{d}(k) = (J_x, 0, J_z \cos k), \quad (11a)$$

$$\vec{d}'(k) = (J_x \cos k, J_x \sin k, J_z). \quad (11b)$$

The vectors  $\vec{n}(k)$  and  $\vec{n}'(k)$  are parallel and anti-parallel for  $k = 0$  and  $k = \pi$ , respectively, and using Eq. (8), it can be seen that the DCN is quantized to one, again reflecting the presence of skyrmion configurations of  $\vec{n}_P(k, t)$  in half of the momentum-time zone. We see that this DCN quantization does not correspond to any topological property of the pre- and post-quench Hamiltonian. Indeed the pre-quench Hamiltonian has a chiral symmetry but it cannot host any topological phase (the winding number is always zero), whereas the post-quench Hamiltonian corresponds to a flat-band Rice-Mele model [57] with a finite imbalance  $J_z$  which prevents the model to have any protecting symmetry. As we show in Fig. 2(a), there are no ESCs, while it is easy to see that DQPTs occurs when  $t^* = (2m+1)\pi/\sqrt{J_x^2 + J_z^2}$  (see Fig. 2(b)). It is worth to point out that a similar case can happen also for quenches within the same AZ class. Considering for example class AIII, in Ref. [50] it was dis-

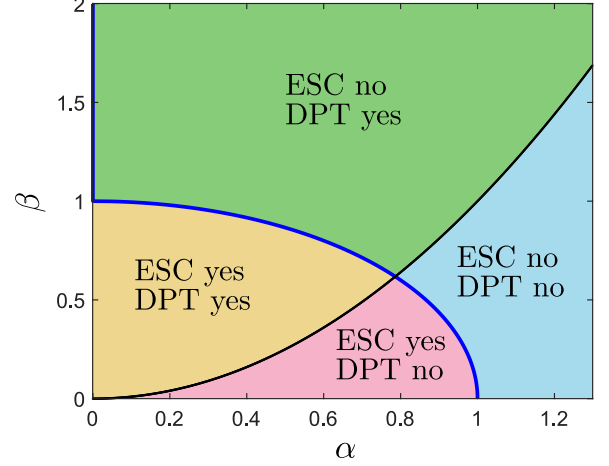


FIG. 3. For the quench protocol  $\vec{d}(k) = J(\beta, 0, \alpha)$  to  $\vec{d}'(k) = J(\cos k, \sin k, \alpha)$ , the parameters  $\alpha$  and  $\beta$  determine the existence of four regions where DQPTs and/or ESCs appear or do not appear. The existence of ESCs extends to the blue line as well (and thus for any  $\alpha = 0$ ), which corresponds to the case of DCN quantized to one.

cussed how the ESCs became unstable under band dispersion of the post-quench Hamiltonian, despite quenching from a trivial to a topological phase, which implies a quantized DCN [41] (and the presence of DQPTs, as we will see below). This exemplifies the fact that the  $(1+1)$ -dimensional topology of the parent Hamiltonian, measured by the DCN, in general does not reflect its 1-dimensional topology, which via bulk-boundary correspondence would become apparent as a degenerate entanglement spectrum.

### 3. Absence of DQPTs

This case cannot exist. In order to have a non-zero quantized DCN, we must have a fixed  $k^*$  inside the Brillouin zone such that  $\vec{n}(k)$  and  $\vec{n}'(k)$  are parallel, i.e.  $\vec{n}(k^*) \cdot \vec{n}'(k^*) = 1$  and a fixed  $k^{**}$  such that  $\vec{n}(k)$  and  $\vec{n}'(k)$  are anti-parallel, i.e.  $\vec{n}(k^{**}) \cdot \vec{n}'(k^{**}) = -1$ . However, since the function  $\vec{n}(k) \cdot \vec{n}'(k)$  must be continuous there must be a  $\bar{k}$  such that  $\vec{n}(\bar{k}) \cdot \vec{n}'(\bar{k}) = \vec{d}(\bar{k}) \cdot \vec{d}'(\bar{k}) = 0$ . This last equality implies the existence of a DQPT. For this reason, we observe that a quantized DCN is a sufficient (but not necessary) condition to have a DQPT.

### B. Vanishing dynamical Chern number

The last four cases reported in Table I can be addressed by studying quantum quenches described by the following

Bloch vectors:

$$\vec{d}(k) = (J_x, 0, J_z) \equiv J(\beta, 0, \alpha), \quad (12a)$$

$$\vec{d}'(k) = (J \cos k, J \sin k, J_z) \equiv J(\cos k, \sin k, \alpha), \quad (12b)$$

where we set  $J_x = \beta J$  and  $J_z = \alpha J$ , with  $\alpha > 0$  and  $\beta > 0$  being dimensionless parameters. Since the vectors  $\vec{n}(k)$  and  $\vec{n}'(k)$  can never be anti-parallel, the DCN is vanishing for all  $\alpha$  and  $\beta$ . This can be also checked by explicitly computing the DCN from Eq. (7), integrating over the whole momentum-time zone  $[-\pi, \pi) \times [0, T)$  with  $T = \frac{\pi}{J\sqrt{1+\alpha^2}}$ : The result vanishes for any  $\alpha$  and  $\beta$ , reflecting the fact that the parent Bloch vector  $\vec{n}_P(k, t)$  does not wrap around the Bloch sphere. DQPTs occur (do not occur) when  $|\alpha^2/\beta| < 1$  ( $|\alpha^2/\beta| > 1$ ). As shown in Fig. 3, DQPTs and ESCs are completely independent. Indeed, by varying the parameters  $\alpha$  and  $\beta$ , there exist four regions where any combination of the presence or absence of these features appears.

### 1. Entanglement spectrum crossings and zero-energy modes

In the previous paragraph we have shown that for a proper choice of the parameters  $\alpha$  and  $\beta$  the parent Hamiltonian exhibits ESCs, i.e. degeneracies of the entanglement spectrum at certain times. We now investigate in more details how such crossings are related to the presence of zero-energy modes. Preliminarily, we observe that for  $\alpha = 0$  and  $\beta = 1$  we recover the phenomenology studied in Subsection III A 1, with non-zero DCN. In particular, the emerging ESCs are associated to the zero-energy modes of a generalized SSH model with next-nearest-neighbor hopping terms supporting four zero-energy modes protected by a chiral symmetry. This result can be easily extended to the case  $\beta \neq 1$ .

We first notice that for  $\alpha < 1$  and  $\beta = 0$ , the emerging ESCs are associated to the zero-energy modes of a standard SSH model with nearest-neighbor hopping terms (see Appendix A 3). In this case, the DCN is zero, however we obtain a non-trivial 1-dimensional topology of the parent Hamiltonian despite quenching between two topologically trivial models.

We now discuss the ESCs appearing for  $\alpha \neq 0$  and  $\beta \neq 0$  and we show that such crossings capture the presence of *accidental* zero-energy modes, i.e. zero-energy modes which are not associated to a standard symmetry protected topological phase. We proceed as follows. First we calculate the vector  $\vec{d}_P(k, t)$  from Eq. (3) for the quantum quench defined in Eq. (12) (see Eq. (A12) in Appendix A 3 for a detailed expression). The corresponding parent Hamiltonian  $h_P(k, t)$  can be written as:

$$h_P(k, t) = h_P^{(n.)}(k, t) + h_P^{(n.n.)}(k, t), \quad (13)$$

with:

$$h_P^{(n.n.)}(k, t) = \begin{pmatrix} 0 & \eta(t)e^{-2ik} \\ \eta^*(t)e^{2ik} & 0 \end{pmatrix}, \quad (14a)$$

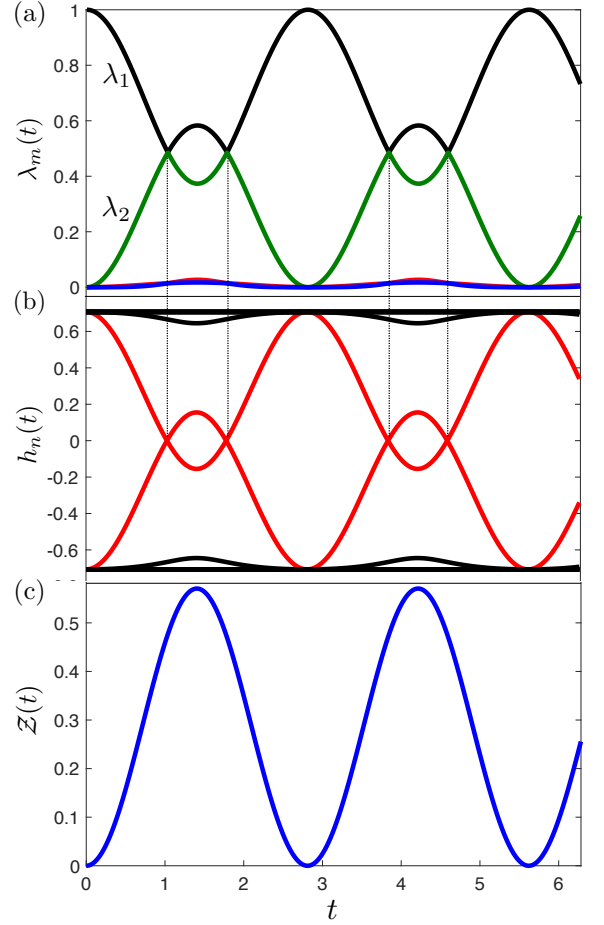


FIG. 4. Quench protocol:  $\vec{d}(k) = J(\beta, 0, \alpha)$  and  $\vec{d}'(k) = J(\cos k, \sin k, \alpha)$  with  $\alpha = \beta = 0.5$  and  $J = 1$ . (a) Time evolution of the entanglement spectrum  $\lambda_m(t)$  of the parent Hamiltonian  $h_P(k, t)$ . (b) Time evolution of the eigenvalues  $h_n(t)$  of the parent Hamiltonian  $\hat{H}_P(t)$  with open boundary conditions. Zero-energy modes appear when the entanglement spectrum is degenerate. (c) Time evolution of the Zak phase of the parent Hamiltonian  $h_P(k, t)$ .

$$h_P^{(n.)}(k, t) = \begin{pmatrix} M(k, t) & \delta(t) + \epsilon(t)e^{-ik} \\ \delta^*(t) + \epsilon^*(t)e^{ik} & -M(k, t) \end{pmatrix}, \quad (14b)$$

with  $M(k, t) = m(t) + m_c(t) \cos k + m_s(t) \sin k$ . The explicit expressions of the functions  $\delta(t)$ ,  $\epsilon(t)$ ,  $\eta(t)$ , and  $M(k, t)$  can be found in Appendix A 3. Given the parent Hamiltonian in momentum space we can easily obtain the parent Hamiltonian in real space, where we notice that  $h_P^{(n.)}(k, t)$  contains on-site terms plus nearest-neighbor hopping terms while  $h_P^{(n.n.)}(k, t)$  contains next-nearest-neighbor hopping contributions. By diagonalizing  $\hat{H}_P(t)$  with open boundary conditions, we observe that zero-energy modes appear in its single-particle spectrum at the times when crossings in the entanglement spectrum happen. This is clear from Fig. 4(a) where we show the occurrence of ESCs accompanied by the appearance of

(pairs of) zero-energy modes in the single-particle spectrum at the same times, shown in Fig. 4(b). A natural question which arises is whether these zero-energy modes are associated to a symmetry protected topological phase.

According to the Altland-Zirnbauer (AZ) classification of topological phases of matter, in one dimension, symmetry protected topological phases with zero-energy modes can appear in the presence of a chiral symmetry  $S$  such that  $S h_P(k, t) S^\dagger = -h_P(k, t)$  (symmetry classes BDI and AIII) or in the presence of a particle-hole symmetry  $C$  such that  $C h_P^*(k, t) C^\dagger = -h_P(-k, t)$  (symmetry class D). Since the matrix  $S$  must be  $k$ -independent, we observe that  $S h_P(k, t) S^\dagger = -h_P(k, t)$  must hold for  $h_P^{(n.)}(k, t)$  and  $h_P^{(n.n.)}(k, t)$  separately, i.e.:  $S h_P^{(n.)}(k, t) S^\dagger = -h_P^{(n.)}(k, t)$  and  $S h_P^{(n.n.)}(k, t) S^\dagger = -h_P^{(n.n.)}(k, t)$ . Hence the zero-energy modes emerging during the time-evolution are not protected by the chiral symmetry. We can indeed define a chiral symmetry  $S = \sigma_z$  for the Hamiltonian  $h^{(n.n.)}(k, t)$ , however one can immediately see that this is not a chiral symmetry for  $h_P^{(n.)}(k, t)$ . We furthermore also checked the absence of any inversion symmetry. Additionally, we also calculate the Zak phase of  $h_P(k, t)$  during the time-evolution, defined as [58, 59]:

$$\mathcal{Z}(t) = i \int_{-\pi}^{\pi} dk \langle u_v(k; t) | \partial_k u_v(k; t) \rangle, \quad (15)$$

where  $|u_v(k; t)\rangle$  denotes the Bloch state of the lower band of  $h_P(k, t)$ , and we observe that it is not quantized when the zero-energy modes appear, as can be seen in Fig. 4(c). We now show that, as long as  $\alpha \neq 0$  and  $\beta \neq 0$ , these emerging zero-energy modes are determined by a fine tuning of the parameters in the parent Hamiltonian  $h_P(k, t)$  and cannot be understood as standard zero-energy modes of a symmetry protected topological phase belonging to a fixed symmetry class of the AZ classification. To this aim, we first observe that the off-diagonal terms of  $h_P(k, t)$  describe a generalized SSH model with nearest- and next-nearest-neighbor terms, and a chiral symmetry  $S = \sigma_z$ . Assuming for the moment the diagonal terms to be equal to zero, the generalized SSH model can host four, two or zero exponentially localized zero-energy modes depending on the values of  $\eta(t)$ ,  $\epsilon(t)$ , and  $\delta(t)$ . Let us now consider a fixed time  $t^*$  at which we have ESCs, e.g.  $t^* = 1.02891$  in the case of  $\alpha = \beta = 0.5$ . In this case the off-diagonal terms alone,  $\eta(t^*)$ ,  $\epsilon(t^*)$ , and  $\delta(t^*)$ , would determine the presence of two zero-energy modes protected by the chiral symmetry  $\sigma_z$ . The presence of diagonal terms breaks this chiral symmetry and generally would split these modes away from zero energy, still preserving their exponentially localized nature. However at time  $t^*$  the interplay of  $m(t^*)$ ,  $m_c(t^*)$ , and  $m_s(t^*)$  constitutes a *fine-tuning* of diagonal elements which restores the two-fold degeneracy of the single-particle spectrum at zero energy, even though no chiral symmetry is present. These modes have therefore

an underlying topological origin, coming from the generalized SSH model in absence of the diagonal terms, but their degeneracy at zero energy is a result of a particular choice of symmetry-breaking terms. This explicates the origin of the ESCs observed in the post-quench dynamics of one-dimensional systems considered here.

#### IV. INTERACTING QUENCH DYNAMICS

In this Section, by means of time-dependent DMRG, we study quench protocols in the presence of a Hubbard repulsive interaction  $U \sum_j \hat{n}_{j,a} \hat{n}_{j,b}$ , with  $\hat{n}_{j,a} = \hat{a}_j^\dagger \hat{a}_j$  and  $\hat{n}_{j,b} = \hat{b}_j^\dagger \hat{b}_j$  for one-dimensional two-band models. This Section is divided into two paragraphs. In the first one, we consider the quench protocol defined in Eq. (12) in the regime where  $\alpha$  and  $\beta$  are tuned to have both DQPTs and ESCs in the non-interacting case and we show that the Hubbard interaction plays a detrimental role to their presence, in the sense that DQPTs and ESCs disappear when  $U$  becomes sufficiently large. In the second paragraph, we investigate the opposite scenario, i.e. we show that DQPTs and ESCs can be generated by performing a quench of the interaction term. Our analysis is performed on an interacting SSH model in the flat band regime which can be addressed both numerically and analytically. The following numerical simulations have been performed using the ITensor library [<http://itensor.org>].

##### A. DQPTs and ESCs in the presence of interactions

We consider the quench protocol defined in Eq. (12) in the regime where  $\alpha = \beta = 0.5$  such that, in the non interacting case, we have both DQPTs and ESCs. We switch on the repulsive Hubbard interaction  $U$  in the post-quench Hamiltonian, albeit we notice that this is equivalent to the case of having it switched on from the very beginning, being it  $SU(2)$  invariant and since we start from a fully polarized state. In Fig. 5 we start investigating the time-evolution of the four largest eigenvalues  $\lambda_m(t)$  of the entanglement spectrum for different values of the Hubbard interaction  $U$  (panels (a) and (b)). Preliminarily we observe that, because of the presence of interactions, the time-evolution is not periodic anymore and many eigenvalues of the entanglement spectrum become non-vanishing during the dynamics. In the presence of weak repulsive interactions, cf. Fig. 5(a), the entanglement spectrum crossings between the two largest eigenvalues are preserved, while they disappear for stronger interactions, cf. Fig. 5(b). In Fig. 5(c), we investigate the degeneracies of the entanglement spectrum at time  $t = t^*$  for which we have a crossing between the two largest eigenvalues at  $U = 0.5J$ , cf. Fig. 5(a). Interestingly, we observe that only the two largest eigenvalues are degenerate, while the lowest ones are not. This is in stark contrast with the non-interacting case for which

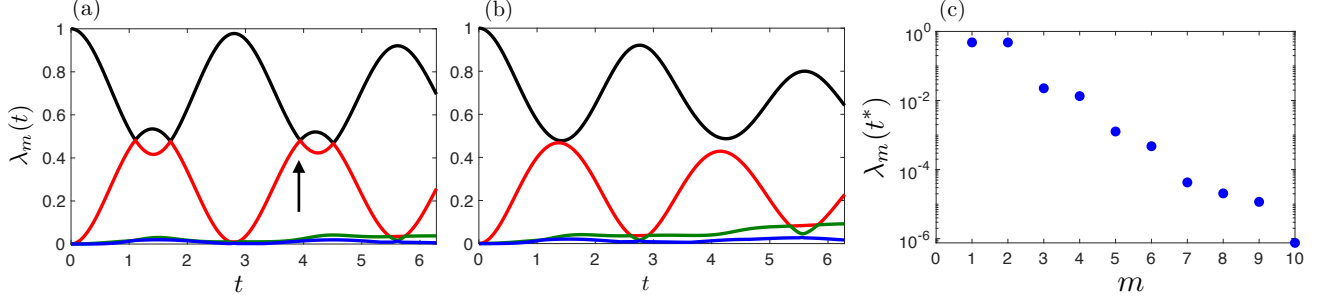


FIG. 5. Time-evolution of the four largest eigenvalues  $\lambda_m(t)$  of the entanglement spectrum for the quench protocol:  $\vec{d}(k) = J(\beta, 0, \alpha)$  and  $\vec{d}'(k) = J(\cos k, \sin k, \alpha)$  with  $\alpha = \beta = 0.5$  and different values of the Hubbard interaction term:  $U = 0.5J$  (a),  $U = J$  (b). (c) The entanglement spectrum at a fixed time  $t^*$  [see the black arrow in (a)] for which we have crossings between the two largest eigenvalues at  $U = 0.5J$ . Data obtained with DMRG for a chain of  $L = 96$  unit cells with OBC and  $J = 1$ , using time step  $dt = 0.0025$  (in units  $1/J$ ). The truncation error is smaller than  $10^{-12}$  at all times.

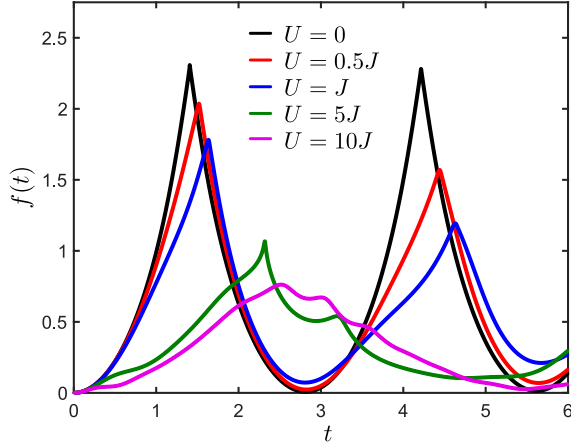


FIG. 6. The rate function  $f(t)$  for the quantum quench  $\vec{d}(k) = J(\beta, 0, \alpha)$  and  $\vec{d}'(k) = J(\cos k, \sin k, \alpha)$  with  $\alpha = \beta = 0.5$  for different values of the Hubbard interaction term  $U$ . Data obtained with DMRG for a chain of  $L = 96$  unit cells with OBC and  $J = 1$ , using time step  $dt = 0.001$ . The truncation error is smaller than  $10^{-12}$  at all times.

the entanglement spectrum is fully degenerate. We have verified that this is not a finite size effect by increasing the size of the system up to  $L = 244$  sites.

In Fig. 6 we show the behavior of the rate function  $f(t)$  for different values of the interaction term. Similarly to the ESCs case, we observe that the divergences of the rate function  $f(t)$  persist in the weakly interacting regime, while they disappear for larger interaction strengths, up to the timescales that we have investigated. We finally mention that the phenomenology observed here is qualitatively unaltered if we set  $\alpha = 0$ , namely considering the case of a quench of the form (9a)-(9b) in the SSH model.

## B. Interacting SSH model

As a different scenario compared to what discussed before, here we consider interaction quenches in an interacting SSH model:

$$\hat{H} = \sum_j \left[ \left( J \hat{a}_{j+1}^\dagger \hat{b}_j + J' \hat{a}_j^\dagger \hat{b}_j + \text{H.c.} \right) + U \hat{n}_{j,a} \hat{n}_{j,b} \right], \quad (16)$$

which supports at half-filling (the particle number  $N$  is equal to the number of sites  $L$ ) a symmetry protected topological phase for  $U < U_c$  and a trivial phase for  $U > U_c$  with  $U_c = 4J$  when  $J' = 0$ . The full phase diagram has been studied in Ref. [60]. In the following, for simplicity, we set  $J' = 0$  and assume to prepare the system in a trivial state by choosing the pre-quench interaction  $U > U_c$ , and quench into the topological phase  $U' < U_c$ . We study this quantum quench protocol — that does not have a counterpart in the non-interacting regime in the sense that the single-particle hopping terms remain constant — numerically assuming open boundary conditions (OBC) and analytically assuming periodic boundary conditions (PBC). We start our analysis assuming PBC and we discuss the existence of DQPTs. To this aim, we introduce the bond operators:

$$\begin{cases} \hat{w}_{j,+} = \frac{1}{\sqrt{2}} \left( \hat{a}_{j+1} + \hat{b}_j \right) \\ \hat{w}_{j,-} = \frac{1}{\sqrt{2}} \left( \hat{a}_{j+1} - \hat{b}_j \right) \end{cases}, \quad (17)$$

and define the  $\mathfrak{su}(2)$  algebra operators:

$$\hat{T}_j^{(x)} = \hat{w}_{j,+}^\dagger \hat{w}_{j,-} + \hat{w}_{j,-}^\dagger \hat{w}_{j,+}, \quad (18a)$$

$$\hat{T}_j^{(y)} = -i(\hat{w}_{j,+}^\dagger \hat{w}_{j,-} - \hat{w}_{j,-}^\dagger \hat{w}_{j,+}), \quad (18b)$$

$$\hat{T}_j^{(z)} = \hat{w}_{j,+}^\dagger \hat{w}_{j,+} - \hat{w}_{j,-}^\dagger \hat{w}_{j,-}, \quad (18c)$$

satisfying the usual commutation relations  $[\hat{T}_i^{(\alpha)}, \hat{T}_j^{(\beta)}] = 2i\epsilon_{\alpha\beta\gamma} \hat{T}_i^{(\gamma)} \delta_{ij}$ . Then, we can map the Hamiltonian (16)



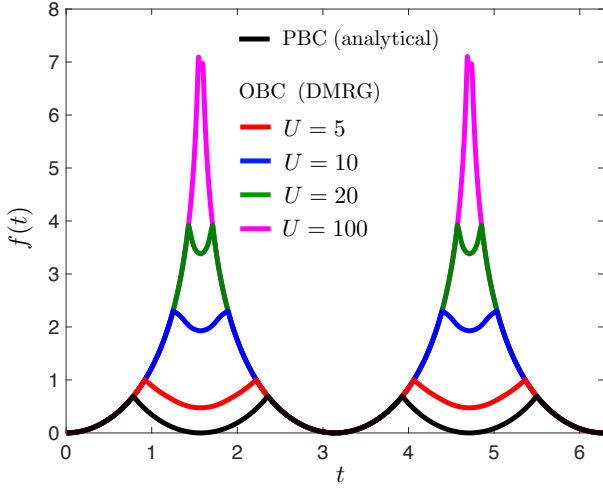


FIG. 7. Time evolution of the rate function  $f(t)$  after a quench in the interacting SSH model from finite (large)  $U$  to  $U' = 0$ . Black line:  $f(t)$  from Eq. (6), valid for PBC, for a quench from  $U = 10J$  to  $U' = 0$ . Red, blue, green and violet lines show  $f(t)$  from DMRG simulations with OBC, for a quenches to  $U' = 0$  starting from  $U = 5J, 10J, 20J$  and  $100J$ , respectively. In the plot  $J = 1$ ,  $L = 1056$ , the time step  $dt = 0.0025$  (in units  $1/J$ ). The truncation error is smaller than  $10^{-12}$  at all times.

onto an Ising chain in the presence of a transverse magnetic field [60]:

$$\hat{H} = \sum_j \left[ J \hat{T}_j^{(z)} - \frac{U}{4} \hat{T}_{j-1}^{(x)} \hat{T}_j^{(x)} \right], \quad (19)$$

and observe that the paramagnetic (anti-ferromagnetic) phase of the Ising chain corresponds to the topological (trivial) phase of the interacting SSH model. Using a standard Jordan-Wigner transformation, the Hamiltonian (19) can be mapped onto a Kitaev chain. If we define  $\hat{c}_i = \hat{S}_{i-1} \hat{T}_i^-$  and  $\hat{c}_i^\dagger = \hat{T}_i^+ \hat{S}_{i-1}$  with  $\hat{T}_j^\pm = (\hat{T}_j^{(x)} \pm i \hat{T}_j^{(y)})/2$  and  $\hat{S}_{i-1} = \prod_{j=1}^{i-1} e^{i\pi \hat{T}_j^+ \hat{T}_j^-}$  the usual string operator, we obtain:

$$\hat{H} = 2J \sum_i \hat{c}_i^\dagger \hat{c}_i - \frac{U}{4} \sum_i (\hat{c}_i^\dagger - \hat{c}_i)(\hat{c}_{i+1}^\dagger - \hat{c}_{i+1}). \quad (20)$$

Using the Nambu spinors  $\hat{C}_k^\dagger = (\hat{c}_k^\dagger \ \hat{c}_{-k})$  in the momentum space representation, we can rewrite the Hamiltonian (20) as  $\hat{H} = \sum_{k>0} \hat{C}_k^\dagger h(k) \hat{C}_k$ , where  $h(k) = \vec{d}(k) \cdot \vec{\sigma}$ , with  $\vec{d}(k) = (0, -U/2 \sin k, 2J - U/2 \cos k)$ ; similarly the vector  $\vec{d}(k)$  corresponding to the post-quench Hamiltonian is  $\vec{d}(k) = (0, -U'/2 \sin k, 2J - U'/2 \cos k)$ . From now on, for simplicity, we set  $J = 1$ .

Before addressing the presence of DQPTs, we observe that, despite the presence of interactions, we are able to map the interacting SSH Hamiltonian (16) onto a quadratic Hamiltonian. Then, using Eq. (8), we can define a DCN for our quench protocol. In particular, the

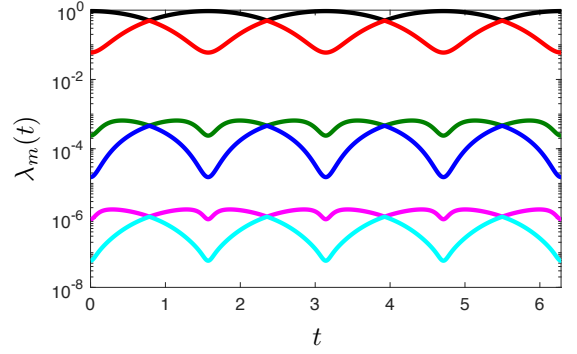


FIG. 8. Time-evolution of the six largest eigenvalues  $\lambda_m(t)$  of the entanglement spectrum for a quench in the interacting SSH model from  $U = 5J$  to  $U' = 0$  with  $J = 1$ . Data obtained with DMRG on a chain of  $L = 1056$  unit cells with OBC, with time step  $dt = 0.0025$  (in units  $1/J$ ). The truncation error is smaller than  $10^{-12}$  at all times.

DCN is equal to one when the pre- and the post-quench Hamiltonian belong to two different phases and vanishes when they belong to the same phase. The existence of DQPTs with PBC can be then diagnosed using Eq. (6) applied to the Kitaev model obtained after the transformations (17) and (18). In the following we assume  $U' = 0$  and observe that DPTs occur when  $t^* = \pi/4 + n\pi/2$ , see the red line data in Fig. (7), as long as  $U > U_c$ .

Using time-dependent DMRG with OBC we have studied the behavior of the rate function  $f(t)$  defined in Eq. (5) by explicitly simulating the quench protocol for the Hamiltonian (16) for  $U' = 0$  and different values of  $U$ . In Fig. 7 we compare our numerical DMRG data with the analytical prediction obtained using Eq. (6). We notice that the rate function  $f(t)$  obtained from DMRG exhibits DQPTs, but not in correspondence of the times  $t^*$  obtained by means of Eq. (6) which is valid with PBC. This discrepancy is a direct consequence of the open boundary conditions and it is not a finite-size effect. As explained in detail in Appendix B, the rate function  $f(t)$  can be calculated analytically with OBC in the limit where  $U' \rightarrow +\infty$ , and is expected to exhibit DQPTs at  $t^* = \pi/2 + n\pi$ . This is in agreement with our DMRG simulations. For smaller values of  $U$ , DQPTs appear at different times. Finally, we study the time evolution of the eigenvalues of the entanglement spectrum. Since the mapping of the fermionic SSH model Eq. (16) in the case  $J' = 0$  to a transverse-field Ising model (IV B) is non-local, as it makes use of the bond operators (17), the time evolution of the eigenvalues of the entanglement spectrum cannot be understood by exploiting this equivalence between the interacting SSH model and the Ising Hamiltonian. Therefore we explicitly simulate the time evolution of the interacting SSH model using DMRG and observe the appearance of entanglement spectrum crossings when quenching from the trivial to the topological phase. The results are shown in Fig. 8, for a quench from  $U = 5J$  to  $U' = 0$ .

## V. CONCLUDING DISCUSSION

In summary, we have investigated the relations between entanglement spectrum crossings (ESCs), dynamical quantum phase transitions (DQPTs) and quantized dynamical Chern number (DCN) in one-dimensional two-band models after a general quantum quench (i.e. not restricted to a given AZ class). In the case of non-interacting systems, we devised quench protocols after which basically any combination between ESCs, DQPTs and quantized DCN can occur (apart from the case of a quantized DCN without DQPTs — see Table I). While the absence of a one-to-one correspondence between these indicators had been previously discussed, here we showed that for general quenches also their relation to topology is in some cases lost. In particular, we were able to generate a finite DCN (see Sec. III A 2) or topological ESCs (see Sec. III B with  $\beta = 0$  and  $\alpha < 1$ ) from topologically trivial Hamiltonians, as well as *accidental* ESCs related to zero-energy boundary modes not protected by a conventional symmetry. Going beyond non-interacting systems, we also investigated the robustness of ESCs and DQPTs to the presence of repulsive Hubbard interactions: While DQPTs are found to persist up to moderate interaction strengths, the full degeneracy of the entanglement spectrum at the crossings does not strictly survive even at small interactions, hinting at the absence of zero-energy boundary modes in the parent Hamiltonian. Finally, we have considered interaction quenches in a SSH model showing, by means of DMRG simulations complemented by an analytical mapping onto a Ising chain in a transverse field, how ESCs and DQPTs can arise for such protocols.

We conclude by pointing out some possible future directions. An interesting point would be investigating the effects of finite temperature (see [61, 62] for a discussion in the context of DQPTs) in such quench problems: Can one identify indicators of some emergent topological property, for example based on the observation of the entanglement spectrum, in the time-evolution after quenches with thermal states? Finally, our results raise the natural question of whether there is a more general way of understanding the appearance of the above signatures for quench protocols not constrained to a single AZ class. This question is of course relevant also beyond the realm of one-dimensional systems studied in this work.

## ACKNOWLEDGMENTS

We acknowledge discussions with Jorge Cayao and Max McGinley. L.P. and J.C.B. acknowledge financial support from the DFG through SFB 1143 (Project No. 247310070). S.B. acknowledges the Hallwachs-Röntgen Postdoc Program of ct.qmat for financial support. Our numerical calculations were performed on resources at the TU Dresden Center for Information Services and High Performance Computing (ZIH).

## Appendix A: Quench Dynamics

In this Appendix we review how the entanglement spectrum, and dynamical quantum phase transitions can be calculated in one-dimensional two-band models. We furthermore provide the explicit expression of the parent Hamiltonian for the quench protocol considered in section III B.

### 1. Entanglement spectrum

We show how to calculate the entanglement spectrum for a non-interacting fermionic system [54, 55]. Without loss of generality we consider a one-dimensional system, as studied in the main text, but the discussion can be easily generalized to higher dimensions. We consider a quadratic Hamiltonian  $\hat{H} = \sum_{i,j=1}^L \hat{c}_i^\dagger H_{ij} \hat{c}_j$ , where  $\hat{c}_i$  is a fermionic operator which annihilates a fermion at site  $i$ . The physical properties of a non-interacting system can be calculated by using only the single-particle density matrix, which has elements  $C_{ij} = \langle \Psi | \hat{c}_i^\dagger \hat{c}_j | \Psi \rangle$ , with  $|\Psi\rangle$  being the state of the system. In the following we discuss how to calculate the von Neumann entropy from the knowledge of the single-particle density matrix. The reduced density matrix  $\hat{\rho}_S$  for a subsystem  $S$  of length  $\ell < L$  can be written as:

$$\hat{\rho}_S = \frac{e^{-\hat{h}_S}}{Z_S} \quad \text{with} \quad Z_S = \text{Tr} \left[ e^{-\hat{h}_S} \right], \quad (\text{A1})$$

where, for a non-interacting system, the *entanglement Hamiltonian*  $\hat{h}_S$  is quadratic in the fermionic operators, i.e.  $\hat{h}_S = \sum_{i,j=1}^\ell \hat{c}_i^\dagger h_{ij} \hat{c}_j$ . By introducing the operators  $\hat{d}_m$  which diagonalize  $\hat{h}_S$ , i.e.  $\hat{h}_S = \sum_{m=1}^\ell \epsilon_m \hat{d}_m^\dagger \hat{d}_m$  with  $\hat{c}_j = \sum_{m=1}^\ell V_{j,m} \hat{d}_m$ , we can express  $\hat{\rho}_S$  as:

$$\hat{\rho}_S = \prod_{m=1}^\ell \frac{e^{-\epsilon_m \hat{d}_m^\dagger \hat{d}_m}}{1 + e^{-\epsilon_m}}, \quad (\text{A2})$$

from which we can see that for  $j, k$  being lattice sites in subsystem  $S$ , we have:

$$\text{Tr}_S \left[ \hat{\rho}_S \hat{c}_j^\dagger \hat{c}_k \right] = \sum_n \frac{V_{j,n}^* V_{k,n}}{1 + e^{\epsilon_n}}. \quad (\text{A3})$$

This gives us a direct relation between the eigenvalues  $\epsilon_n$  of the entanglement Hamiltonian and the eigenvalues of the single-particle density matrix restricted to subsystem  $S$ . Namely, denoting with  $\xi_n$  the eigenvalues of the single-particle density matrix reduced to  $S$ , we have:

$$\xi_n = \frac{1}{1 + e^{\epsilon_n}}. \quad (\text{A4})$$

It is therefore sufficient to diagonalize the single-particle density matrix restricted to subsystem  $S$  for knowing the eigenvalues  $\epsilon_n$  of the entanglement Hamiltonian  $\hat{h}_S$ , from

which we can calculate the eigenvalues of the reduced density matrix  $\hat{\rho}_S$  as:

$$\lambda_{\{s_m\}} = \prod_{m=1}^{\ell} \left[ \frac{1}{2} + s_m \left( \xi_m - \frac{1}{2} \right) \right] \quad \text{with } s_m = \pm 1. \quad (\text{A5})$$

In particular, the highest entanglement spectrum eigenvalue would correspond to occupying all the lowest eigenstates of  $\hat{h}_S$  with energy  $\epsilon_m < 0$ , i.e.  $\xi_m > 1/2$ , by setting  $s_m = 1$  for them, and leaving the remaining ones empty with  $s_m = -1$ . The other eigenvalues are simply computed as excitations above this Fermi sea.

## 2. Dynamical phase transitions

DQPTs are hallmarked by divergences of the rate function:

$$f(t) = - \lim_{L \rightarrow +\infty} \frac{1}{L} \ln[\mathcal{L}(t)], \quad (\text{A6})$$

associated to the Loschmidt echo  $\mathcal{L}(t) = |\langle \Psi | e^{-i\hat{H}'t} | \Psi \rangle|^2$ , where  $|\Psi\rangle$  is the initial quantum state. In this Appendix we briefly discuss under which conditions a DQPT can appear in two-band systems. To this end, we recall that the pre-quench Hamiltonian  $\hat{H} = \sum_k \hat{\Pi}_k^\dagger h(k) \hat{\Pi}_k$ , with  $h(k) = \vec{d}(k) \cdot \vec{\sigma}$ , can be diagonalized in momentum space by a unitary matrix  $M_k$  such that  $M_k^\dagger h(k) M_k = E(k) \sigma_z$ , yielding  $\hat{H} = \sum_k E(k) \hat{\Phi}_k^\dagger \sigma_z \hat{\Phi}_k$  with  $\hat{\Phi}_k^\dagger = \Pi_k^\dagger M_k = (\hat{c}_{k,U}^\dagger, \hat{c}_{k,L}^\dagger)$ . Similarly, the parent Hamiltonian  $\hat{H} = \sum_k \hat{\Pi}_k^\dagger h_P(k, t) \hat{\Pi}_k$  is diagonalized at each time  $t$  by a matrix  $M_k(t)$  such that  $\hat{H}_P = \sum_k E(k) \hat{\Phi}_k^\dagger(t) \sigma_z \hat{\Phi}_k(t)$ , with  $\hat{\Phi}_k^\dagger(t) = \Pi_k^\dagger M_k(t) = (\hat{c}_{k,U}^\dagger(t), \hat{c}_{k,L}^\dagger(t))$ . Taking the initial state  $|\Psi\rangle$  as the ground-state of  $\hat{H}$ , we can express the initial and the time-evolved state as  $|\Psi\rangle = \prod_k \hat{c}_{k,L}^\dagger |0\rangle = \prod_k \hat{\Pi}_k^\dagger U(k) |0\rangle$  and the time-evolved state  $|\Psi(t)\rangle = \prod_k \hat{c}_{k,L}^\dagger(t) |0\rangle = \prod_k \hat{\Pi}_k^\dagger U(k, t) |0\rangle$ , respectively, with the spinors  $U$  defined by  $h(k)U(k) = -E(k)U(k)$  and  $h_P(k, t)U(k, t) = -E(k)U(k, t)$ . Using the definition (A6) we then obtain:

$$f(t) = - \int_{-\pi}^{+\pi} \frac{dk}{2\pi} \ln |U^\dagger(k) U(k, t)|^2, \quad (\text{A7})$$

where we used  $\lim_{L \rightarrow +\infty} 1/L \sum_k \approx - \int_{-\pi}^{+\pi} dk / (2\pi)$ . Defining  $\vec{n}_P(k, t) = -\vec{d}_P(k, t)/d_P(k, t)$  and  $\vec{n}(k) = -\vec{d}(k)/d(k)$  we see that:

$$\begin{aligned} |U(k)^\dagger U(k, t)|^2 &= \text{Tr} \left[ \frac{1 + \vec{n}_P(k, t) \cdot \vec{\sigma}}{2} \frac{1 + \vec{n}(k) \cdot \vec{\sigma}}{2} \right] = \\ &= \frac{1}{2} [1 + \vec{n}_P(k, t) \cdot \vec{n}(k)], \end{aligned} \quad (\text{A8})$$

and using Eq. (4) we finally obtain:

$$f(t) = - \int_{-\pi}^{+\pi} \frac{dk}{2\pi} \ln [\cos^2[d'(k)t] + \gamma(k) \sin^2[d'(k)t]], \quad (\text{A9})$$

with  $\gamma(k) = [\vec{n}'(k) \cdot \vec{n}(k)]^2$ . Singularities of  $f(t)$  come from those momenta  $k^*$  at which  $\gamma(k^*) = 0$ , happening periodically at times  $t^* = (2n+1)\pi/d'(k^*)$ , with  $n \in \mathbb{N}$ .

## 3. Parent Hamiltonian for two-band models

In this Appendix we calculate the explicit expressions (4a)-(4c) for the Hamiltonians:

$$\vec{d}(k) = (J_x, J_y, J_z), \quad (\text{A10a})$$

$$\vec{d}'(k) = (J' + J \cos k, J \sin k, \Delta). \quad (\text{A10b})$$

To this aim we conveniently introduce:

$$\begin{aligned} A(k) &\equiv \frac{[\vec{d}(k) \cdot \vec{d}'(k)]}{d'^2(k)} = \\ &= [(J' + J \cos k)J_x + J J_y \sin k + J_z \Delta] / d'^2(k), \end{aligned} \quad (\text{A11})$$

with  $d'(k) = \sqrt{(J' + J \cos k)^2 + J^2 \sin^2 k + \Delta^2}$  and using Eq. (3) we obtain:

$$d_P^{(x)}(k, t) = A(k)(J' + J \cos k) + \cos[2d'(k)t][J_x - A(k)(J' + J \cos k)] + \sin[2d'(k)t] \frac{J J_z \sin k - \Delta J_y}{d'(k)}, \quad (\text{A12a})$$

$$d_P^{(y)}(k, t) = A(k)J \sin k + \cos[2d'(k)t][J_y - A(k) \sin k] + \sin[2d'(k)t] \frac{\Delta J_x - J_z(J' + J \cos k)}{d'(k)}, \quad (\text{A12b})$$

$$d_P^{(z)}(k, t) = A(k)\Delta + \cos[2d'(k)t][J_z - A(k)\Delta] + \sin[2d'(k)t] \frac{J_y(J' + J \cos k) - J_x J \sin k}{d'(k)}. \quad (\text{A12c})$$

In the case considered in the main text:

$$\vec{d}(k) = J(\beta, 0, \alpha), \quad (\text{A13a})$$

$$\vec{d}'(k) = J(\cos k, \sin k, \alpha), \quad (\text{A13b})$$

we obtain:

$$h_P(k, t) = \vec{d}_P(k, t) \cdot \vec{\sigma} = h_P^{(n.)}(k, t) + h_P^{(n.n.)}(k, t). \quad (\text{A14})$$

In the above equation:

$$h_P^{(n.n.)}(k, t) = \begin{pmatrix} 0 & \eta(t)e^{-2ik} \\ \eta(t)e^{2ik} & 0 \end{pmatrix}, \quad (\text{A15})$$

where:

$$\eta(t) = \frac{\beta J}{1 + \alpha^2} \sin^2(\sqrt{1 + \alpha^2} Jt), \quad (\text{A16})$$

and:

$$h_P^{(n.)}(k, t) = \begin{pmatrix} M(k, t) & \delta(t) + \epsilon(t)e^{-ik} \\ \delta^*(t) + \epsilon^*(t)e^{ik} & -M(k, t) \end{pmatrix} \quad (\text{A17})$$

with the off-diagonal terms being:

$$\epsilon(t) = \frac{\alpha J}{1 + \alpha^2} \left[ \alpha \left( 1 - \cos(2\sqrt{1 + \alpha^2} Jt) \right) + i\sqrt{1 + \alpha^2} \sin(2\sqrt{1 + \alpha^2} Jt) \right], \quad (\text{A18a})$$

$$\delta(t) = \frac{\beta J}{2(1 + \alpha^2)} \left[ 1 + (1 + 2\alpha^2) \cos(2\sqrt{1 + \alpha^2} Jt) + 2i\alpha\sqrt{1 + \alpha^2} \sin(2\sqrt{1 + \alpha^2} Jt) \right], \quad (\text{A18b})$$

and diagonal ones being:

$$M(k, t) = m(t) + m_s(t) \sin k + m_c(t) \cos k, \quad (\text{A18c})$$

$$m(t) = \frac{\alpha J}{1 + \alpha^2} \left[ \alpha^2 + \cos(2\sqrt{1 + \alpha^2} Jt) \right], \quad (\text{A18d})$$

$$m_c(t) = \frac{2J\alpha\beta}{1 + \alpha^2} \sin^2(\sqrt{1 + \alpha^2} Jt), \quad (\text{A18e})$$

$$m_s(t) = -\frac{\beta}{\sqrt{1 + \alpha^2}} \sin(2\sqrt{1 + \alpha^2} Jt). \quad (\text{A18f})$$

In particular, focusing on the case of  $J = 1$  and  $\alpha = \beta = 0.5$ , one can see that, at the time  $t_1^* = 1.02891$  when the ESCs happen for the first time, the Bloch vector for the parent Hamiltonian takes the form:

$$\vec{d}_P(k, t_1^*) = \gamma \begin{pmatrix} 2(\cos k + \sin k) + 2 \cos 2k \\ 1 - 2(\cos k - \sin k) + 2 \sin 2k \\ 2(\cos k - \sin k) - 1 \end{pmatrix}, \quad (\text{A19})$$

with  $\gamma \approx 0.1\bar{6}$ , while at the second time  $t_2^*$  we have  $\vec{d}_P(k, t_2^*) = \vec{d}_P(-k, t_1^*)$ . The spectrum of these models with open boundary conditions have a pair of exponentially localized edge modes at zero energy, although no apparent time-reversal, particle-hole, chiral or inversion symmetry is present.

## Appendix B: Interacting Quench Dynamics

In this Appendix we report details regarding the calculation of dynamical phase transitions in the interacting models considered.

### 1. DQPT in interacting SSH model

Here we consider the quench protocol for the interacting SSH model presented in the Subsection IV B and we discuss how the choice of the boundary conditions affects the times  $t^*$  in correspondence of which DQPTs appear. We recall that the pre- and post-quench Hamiltonians are:

$$\hat{H} = \sum_{j=1}^{L_{BC}} \left( J \hat{a}_{j+1}^\dagger \hat{b}_j + \text{H.c.} \right) + U \sum_{j=1}^L \hat{n}_{j,a} \hat{n}_{j,b}, \quad (\text{B1})$$

and:

$$\hat{H}' = \sum_{j=1}^{L_{BC}} \left( J \hat{a}_{j+1}^\dagger \hat{b}_j + \text{H.c.} \right), \quad (\text{B2})$$

with  $L_{BC} = L$  ( $L_{BC} = L - 1$ ) for periodic (open) boundary conditions. In particular, we discuss the reason why, with open boundary conditions and in the regime  $U \gg J$ , DQPTs appear at  $t^* = \pi/2 + n\pi/2$  (in units of  $J$ ) rather than at  $t^* = \pi/4 + n\pi/2$  as expected with periodic boundary conditions. In the regime  $U \gg J$ , using standard perturbation theory, it is easy to prove that the the ground state of the pre-quench Hamiltonian is doubly degenerate, and the two lowest energy configurations are given by  $|\Psi_A\rangle = \prod_{j=1}^L \hat{a}_j^\dagger |0\rangle$  and  $|\Psi_B\rangle = \prod_{j=1}^L \hat{b}_j^\dagger |0\rangle$ . Because of the inversion symmetry of the SSH Hamiltonian  $\hat{I} = \sigma_x \otimes \hat{R}$  (with  $\hat{R}$  being the spatial reflection and  $\sigma_x$  acting on the sublattice indices), the two degenerate ground states correspond to the symmetric and the anti-symmetric linear combinations  $|\Psi_\pm\rangle = (|\Psi_A\rangle \pm |\Psi_B\rangle)/\sqrt{2}$ . Introducing the bond operators:

$$\begin{cases} \hat{w}_{j,+} = \frac{1}{\sqrt{2}} (\hat{a}_{j+1} + \hat{b}_j) \\ \hat{w}_{j,-} = \frac{1}{\sqrt{2}} (\hat{a}_{j+1} - \hat{b}_j) \end{cases}, \quad (\text{B3})$$

the post-quench Hamiltonian takes the form:

$$\hat{H}' = J \sum_{j=1}^{L-1} \left( \hat{w}_{j,+}^\dagger \hat{w}_{j,+} - \hat{w}_{j,-}^\dagger \hat{w}_{j,-} \right), \quad (\text{B4})$$

consisting of on-site terms only. For convenience we also define the single-particle states  $|j, A\rangle = \hat{a}_j^\dagger |0\rangle$ ,  $|j, B\rangle =$



$\hat{b}_j^\dagger|0\rangle$  and  $|j, +\rangle = \hat{w}_{j,+}^\dagger|0\rangle$  and  $|j, -\rangle = \hat{w}_{j,-}^\dagger|0\rangle$ . We observe that with open boundary conditions,  $j = 1, \dots, L-1$  and the states  $|1, A\rangle$  and  $|L, B\rangle$  are completely decoupled. Since  $|\Psi_A\rangle$  and  $|\Psi_B\rangle$  are Slater determinants, under the action of the non-interacting post-quench Hamiltonian  $\hat{H}'$ , their single-particle states evolve in time as:

$$e^{-i\hat{H}'t}|j, A\rangle = e^{-it}|j-1, +\rangle - e^{it}|j-1, -\rangle, \quad (\text{B5a})$$

for  $j = 1, \dots, L-1$  and:

$$e^{-i\hat{H}'t}|j, B\rangle = e^{-it}|j, +\rangle + e^{it}|j, -\rangle \quad (\text{B5b})$$

for  $j = 2, \dots, L$ . More explicitly we observe that, with open boundary conditions, the states  $|1, A\rangle$  and  $|L, B\rangle$  do not evolve. We now consider the time  $t^* = \pi/2$  and, in order to diagnose the appearance of a DQPT, we calculate the overlap:

$$\begin{aligned} \langle \Psi_\pm | \Psi_\pm(t) \rangle &= \langle \Psi_A | \Psi_A(t) \rangle + \langle \Psi_B | \Psi_B(t) \rangle \pm \\ &\quad + (\langle \Psi_A | \Psi_B(t) \rangle + \langle \Psi_B | \Psi_A(t) \rangle). \end{aligned} \quad (\text{B6})$$

Using Eqs. (B5a)-(B5b), it is easy to prove that:

$$e^{-i\hat{H}'\frac{\pi}{2}}|j, A\rangle = -i|j-1, B\rangle, \quad (\text{B7a})$$

$$e^{-i\hat{H}'\frac{\pi}{2}}|j, B\rangle = -i|j+1, A\rangle. \quad (\text{B7b})$$

Using the fact that for two Slater determinants  $|\Psi\rangle$  and  $|\Phi\rangle$  made of  $L$  single-particle states  $|\psi_j\rangle$  and  $|\phi_j\rangle$  with  $j = 1, \dots, L$ , respectively, their overlap is given by the determinant of the single-particle overlap matrix, i.e.  $\langle \Phi | \Psi \rangle = \det[\langle \phi_i | \psi_j \rangle]_{i,j}$ , we observe that  $\langle \Psi_A | \Psi_A(\pi/2) \rangle = \langle \Psi_B | \Psi_B(\pi/2) \rangle = 0$  with both OBC and PBC. We thus concentrate on  $\langle \Psi_B | \Psi_A(\pi/2) \rangle$  (similar arguments hold for  $\langle \Psi_A | \Psi_B(\pi/2) \rangle$ ). In the case of OBC since  $|1, A\rangle$  remains unchanged, while all other  $|j, A\rangle$  states in  $|\Psi_A\rangle$  shift to  $B$  states, the overlap matrix has a column of zeros and therefore its determinant vanishes. Thus, at  $t^* = \pi/2$  we have  $\langle \Psi_\pm | \Psi_\pm(\pi/2) \rangle = 0$ , which implies a DQPT. On the contrary, with PBC, it is possible to show that  $\langle \Psi_\pm | \Psi_\pm(\pi/2) \rangle = \pm(-1)^{L/2}$ , which implies that the rate function vanishes.

## 2. Calculation of rate function with DMRG

Here we discuss how to practically calculate the rate function  $f(t)$  using matrix product states (MPS) techniques when the system size  $L$  becomes large. When the

initial state  $|\Psi\rangle$  and its time evolved  $|\Psi(t)\rangle$  are expressed as MPS their overlap can be straightforwardly calculated. However, at times  $t^*$  at which we have a DPT we have that the rate function  $f(t)$  defined in Eq. (5) becomes of order one, meaning that  $|\langle \Psi | \Psi(t^*) \rangle|^2 \sim O(e^{-L})$ . For large system sizes the value of  $|\langle \Psi | \Psi(t^*) \rangle|^2$  is thus so small that it cannot be represented on a computer, thus yielding incorrect results. To overcome this problem, we iteratively rescale the overlap during its calculation in the MPS representation, to keep it of order one, and resum the logarithms of the rescaling factors at each step in order to access the rate function at the end of the calculation. Specifically, we calculate  $\tilde{O}(t) = A(t)\langle \Psi | \Psi(t) \rangle$  with  $A(t) = \prod_{j=1}^L \alpha_j(t)$ , where the  $\alpha_j$  are real rescaling parameters chosen such that  $|\tilde{O}(t)| \sim O(1)$ , and in terms of  $\tilde{O}(t)$  the rate function becomes:

$$f(t) = -\frac{1}{L} \log |\tilde{O}(t)|^2 + \frac{2}{L} \sum_{j=1}^L \log \alpha_j(t), \quad (\text{B8})$$

where the first term is now negligible if  $|\tilde{O}(t)| \simeq 1$ . We perform the following choice for the  $\alpha_j(t)$ . For MPS expressed as:

$$|\Psi\rangle = \sum_{\sigma_1, \dots, \sigma_L} M^{[1]\sigma_1} M^{[2]\sigma_2} \dots M^{[L]\sigma_L} |\sigma_1, \sigma_2, \dots, \sigma_L\rangle, \quad (\text{B9})$$

with  $\sigma_j$  denoting the occupation number at site  $j$ , and  $M^{[j]\sigma_j}$  being matrices with elements  $M_{a_{j-1}, a_j}^{[j]\sigma_j}$  (with  $M^{[1]\sigma_1}$  and  $M^{[L]\sigma_L}$  being row and column vectors respectively), and  $|\Psi(t)\rangle$  having the same expression with different matrices  $\tilde{M}$ , the overlap is conveniently calculated by introducing matrices  $C^{[j]}$  whose elements are given by:

$$C_{a_j, a'_j}^{[j]} = \sum_{\sigma_j} (M^{[j]\sigma_j})_{a_j, a_{j-1}}^\dagger C_{a_{j-1}, a'_{j-1}}^{[j-1]} \tilde{M}_{a'_{j-1}, a'_j}^{[j]\sigma_j}, \quad (\text{B10})$$

with  $C^{[0]} = 1$  being the identity [52]. The overlap is then  $\langle \Psi | \Psi(t) \rangle = C^{[L]}$ . We compute the  $\alpha_j$  by rescaling the  $C^{[j]}$  at each step of the computation of the overlap  $C^{[L]}$ , that is for each  $j$ ,  $C^{[j]}$  is replaced by  $\alpha_j C^{[j]}$  where:

$$\alpha_j = \text{tr}[(C^{[j]})^\dagger C^{[j]}]^{-\frac{1}{2}}, \quad (\text{B11})$$

which keep  $|\tilde{O}(t)|$  of order one, therefore avoiding problems related to exponentially small numbers.

- 
- [1] M. Z. Hasan and C. L. Kane, *Rev. Mod. Phys.* **82**, 3045 (2010).
  - [2] X.-L. Qi and S.-C. Zhang, *Rev. Mod. Phys.* **83**, 1057 (2011).
  - [3] X.-G. Wen, *Rev. Mod. Phys.* **89**, 041004 (2017).

- [4] I. Bloch, J. Dalibard, W. Zwerger, *Rev. Mod. Phys.* **80**, 885 (2008).
- [5] N. Goldman, G. Juzeliūnas, P. Öhberg, and I.B. Spielman, *Rep. Prog. Phys.* **77** 126401 (2014).

- [6] M. Aidelsburger, S. Nascimbene, and N. Goldman, *C. R. Physique* **19** (2018) 394-432.
- [7] N. Goldman, J. C. Budich, and P. Zoller, *Nat. Phys.* **12**, 639 (2016).
- [8] A. Eckardt, *Rev. Mod. Phys.* **89**, 011004 (2017.)
- [9] N. R. Cooper, J. Dalibard, and I. B. Spielman *Rev. Mod. Phys.* **91**, 015005 (2019).
- [10] M. S. Rudner and N. H. Lindner, *arXiv:1909.02008*.
- [11] M. Aidelsburger, M. Atala, S. Nascimbene, S. Trotzky, Y.-A. Chen, and I. Bloch, *Phys. Rev. Lett.* **107**, 255301 (2011).
- [12] J. Struck, C. Ölschläger, M. Weinberg, P. Hauke, J. Simonet, A. Eckardt, M. Lewenstein, K. Sengstock, and P. Windpassinger, *Phys. Rev. Lett.* **108**, 225304 (2012).
- [13] J. Struck, M. Weinberg, C. Ölschläger, P. Windpassinger, J. Simonet, K. Sengstock, R. Häppner, P. Hauke, A. Eckardt, M. Lewenstein, and L. Mathey, *Nat. Phys.* **9**, 738 (2013).
- [14] H. Miyake, G. A. Siviloglou, C. J. Kennedy, W. C. Burton, and W. Ketterle, *Phys. Rev. Lett.* **111**, 185302 (2013).
- [15] M. Aidelsburger, M. Atala, M. Lohse, J. T. Barreiro, B. Paredes, and I. Bloch, *Phys. Rev. Lett.* **111**, 185301 (2013).
- [16] G. Jotzu, M. Messer, R. Desbuquois, M. Lebrat, T. Uehlinger, D. Greif, and T. Esslinger, *Nature* **515**, 237 (2014).
- [17] M. Mancini, G. Pagano, G. Cappellini, L. Livi, M. Rider, J. Catani, C. Sias, P. Zoller, M. Inguscio, M. Dalmonte, and L. Fallani, *Science* **349**, 1510 (2015).
- [18] B. K. Stuhl, H. I. Lu, L. M. Aycock, D. Genkina, and I. B. Spielman, *Science* **349**, 1514 (2015).
- [19] A. Bermudez, D. Patane, L. Amico, and M. A. Martin-Delgado, *Phys. Rev. Lett.* **102**, 135702 (2009).
- [20] M. S. Foster, M. Dzero, V. Gurarie, and E. A. Yuzbashyan, *Phys. Rev. B* **88**, 104511 (2013).
- [21] A. Rajak and A. Dutta, *Phys. Rev. E* **89**, 042125 (2014).
- [22] M. D. Caio, N. R. Cooper, and M. J. Bhaseen, *Phys. Rev. Lett.* **115**, 236403 (2015).
- [23] Y. Hu, P. Zoller, and J. C. Budich, *Phys. Rev. Lett.* **117**, 126803 (2016).
- [24] J. H. Wilson, J. C. W. Song, and G. Refael, *Phys. Rev. Lett.* **117**, 235302 (2016).
- [25] P. D. Sacramento, *Phys. Rev. E* **93**, 062117 (2016).
- [26] C. Wang, P. Zhang, X. Chen, J. Yu, and H. Zhai, *Phys. Rev. Lett.* **118**, 185701 (2017).
- [27] L. Barbiero, L. Santos, and N. Goldman, *Phys. Rev. B* **97**, 201115(R) (2018).
- [28] W. Sun, C.-R. Yi, B.-Z. Wang, W.-W. Zhang, B. C. Sanders, X.-T. Xu, Z.-Y. Wang, J. Schmiedmayer, Y. Deng, X.-J. Liu, S. Chen, and J.-W. Pan, *Phys. Rev. Lett.* **121**, 250403 (2018).
- [29] L. Zhang, L. Zhang, S. Niu, and X.-J. Liu, *Sci. Bull.* **63**, 1385 (2018).
- [30] M. McGinley and N. R. Cooper, *Phys. Rev. Lett.* **121**, 090401 (2018).
- [31] M. McGinley and N. R. Cooper, *Phys. Rev. B* **99**, 075148 (2019).
- [32] M. Heyl, A. Polkovnikov, and S. Kehrein, *Phys. Rev. Lett.* **110**, 135704 (2013).
- [33] S. Vajna and B. Dóra, *Phys. Rev. B* **91**, 155127 (2015).
- [34] J. C. Budich and M. Heyl, *Phys. Rev. B* **93**, 085416 (2016).
- [35] N. Sedlmayr, P. Jaeger, M. Maiti, and J. Sirker, *Phys. Rev. B* **97**, 064304 (2016).
- [36] Z. Huang and A. V. Balatsky, *Phys. Rev. Lett.* **117**, 086802 (2016).
- [37] M. Heyl, *Rep. Prog. Phys.* **81**, 054001 (2018).
- [38] G. Torlai, L. Tagliacozzo, and G. De Chiara, *J. Stat. Mech.* P06001 (2014).
- [39] E. Canovi, E. Ercolessi, P. Naldesi, L. Taddia, and D. Vodola, *Phys. Rev. B* **89**, 104303 (2014).
- [40] Z. Gong and M. Ueda, *Phys. Rev. Lett.* **121**, 250601 (2018).
- [41] C. Yang, L. Li, and S. Chen, *Phys. Rev. B* **97**, 060304(R) (2018).
- [42] A. Altland, and M. R. Zirnbauer, *Phys. Rev. B* **55**, 1142 (1997).
- [43] A. P. Schnyder, S. Ryu, A. Furusaki, and A. W. W. Ludwig, *Phys. Rev. B* **78**, 195125 (2008).
- [44] A. W. W. Ludwig, *Phys. Scr.* **T168**, 014001 (2016).
- [45] C. B. Mendl, J. C. Budich, *Phys. Rev. B* **100**, 224307 (2019).
- [46] L. Fidkowski, *Phys. Rev. Lett.* **104**, 130502 (2010).
- [47] F. Pollmann, A. M. Turner, E. Berg, and M. Oshikawa, *Phys. Rev. B* **81**, 064439 (2010).
- [48] A. M. Turner, Y. Zhang, and A. Vishwanath, *Phys. Rev. B* **82**, 241102(R) (2010).
- [49] A. M. Turner, F. Pollmann, and E. Berg, *Phys. Rev. B* **83**, 075102 (2011).
- [50] S. Lu and J. Yu, *Phys. Rev. A* **99**, 033621 (2019).
- [51] S. R. White, *Phys. Rev. Lett.* **69**, 2863 (1992).
- [52] U. Schollwöck, *Ann. Phys.* **326**, 96 (2011).
- [53] W.-P. Su, J. R. Schrieffer, and A. J. Heeger, *Phys. Rev. Lett.* **42**, 1698 (1979).
- [54] G. Vidal, J. I. Latorre, E. Rico, and A. Kitaev, *Phys. Rev. Lett.* **90**, 227902 (2003).
- [55] I. Peschel and V. Eisler, *J. Phys. A: Math. Theor.* **42**, 504003 (2009).
- [56] L. Li, Z. Xu, and S. Chen *Phys. Rev. B* **89**, 085111 (2014).
- [57] M. J. Rice and E. J. Mele *Phys. Rev. Lett.* **49**, 1455 (1982).
- [58] J. Zak, *Phys. Rev. Lett.* **62**, 2747 (1989).
- [59] R. Resta, *J. Phys.: Condens. Matter* **12** R107 (2000).
- [60] J. Jünemann, A. Piga, S.-J. Ran, M. Lewenstein, M. Rizzi, and A. Bermudez, *Phys. Rev. X* **7**, 031057 (2017).
- [61] U. Bhattacharya, S. Bandyopadhyay, and A. Dutta, *Phys. Rev. B* **96**, 180303(R) (2017).
- [62] M. Heyl and J. C. Budich, *Phys. Rev. B* **96**, 180304(R) (2017).